



Compact and cost effective lab-based edge-illumination x-ray phase contrast imaging with a structured focal spot

D. Basta, M. Endrizzi, F. A. Vittoria, A. Astolfo, and A. Olivo

Citation: [Applied Physics Letters](#) **108**, 224102 (2016); doi: 10.1063/1.4953459

View online: <http://dx.doi.org/10.1063/1.4953459>

View Table of Contents: <http://scitation.aip.org/content/aip/journal/apl/108/22?ver=pdfcov>

Published by the [AIP Publishing](#)

Articles you may be interested in

[A laboratory based edge-illumination x-ray phase-contrast imaging setup with two-directional sensitivity](#)
Appl. Phys. Lett. **107**, 204105 (2015); 10.1063/1.4935983

[Image segmentation of nanoscale Zernike phase contrast X-ray computed tomography images](#)
J. Appl. Phys. **117**, 183102 (2015); 10.1063/1.4919835

[Method for automatization of the alignment of a laboratory based x-ray phase contrast edge illumination system](#)
Rev. Sci. Instrum. **84**, 083702 (2013); 10.1063/1.4816827

["Edge illumination" in X-ray Phase Contrast Imaging](#)
AIP Conf. Proc. **1466**, 118 (2012); 10.1063/1.4742279

[Fabrication of large area X-ray diffraction grating for X-ray phase imaging](#)
AIP Conf. Proc. **1466**, 51 (2012); 10.1063/1.4742268

The image shows the cover of an Applied Physics Reviews journal issue. It features a blue and orange color scheme with a molecular structure background. The text 'NEW Special Topic Sections' is prominently displayed in white. Below it, 'NOW ONLINE' is written in yellow, followed by the title 'Lithium Niobate Properties and Applications: Reviews of Emerging Trends' in white. The AIP Applied Physics Reviews logo is in the bottom right corner.

NEW Special Topic Sections

NOW ONLINE
Lithium Niobate Properties and Applications:
Reviews of Emerging Trends

AIP Applied Physics Reviews

Compact and cost effective lab-based edge-illumination x-ray phase contrast imaging with a structured focal spot

D. Basta,^{a)} M. Endrizzi, F. A. Vittoria, A. Astolfo, and A. Olivo

Department of Medical Physics and Bioengineering, University College London, Malet Place, Gower Street, London WC1E 6BT, United Kingdom

(Received 10 March 2016; accepted 22 May 2016; published online 3 June 2016)

We present a different implementation of the Edge Illumination (EI) X-ray Phase Contrast imaging method based on the use of multiple focal spots created through an additional x-ray mask. While this resembles directly inspired by the Talbot-Lau implementation of grating interferometry, the aim of the source mask and its effect on the acquired images are different. The individual “sourcelets” are much larger than in grating methods, and then still spatially incoherent; however, their use allows (a) exploiting cheap and large focal spot sources and (b) reducing the source spot size from the usual 70–100 μm typically used in EI to few tens of μm , which enables the realisation of more compact setups. However, in EI, multiple sources create images shifted by one detector pixel with respect to the other, imposing the use of an image restoration algorithm. Here, we show that the approach is feasible by deconvolving differential phase-contrast image profiles acquired with three separate sources, and comparing results with simulation predictions for equivalent profiles generated by a single source. We also show that this enables reducing the system length from the 2 m used so far to 1 m. © 2016 Author(s). All article content, except where otherwise noted, is licensed under a Creative Commons Attribution (CC BY) license (<http://creativecommons.org/licenses/by/4.0/>). [<http://dx.doi.org/10.1063/1.4953459>]

The potential of X-ray Phase Contrast imaging (XPCI) has been widely explored over recent years, especially in applications where low-absorbing materials are imaged. While XPCI methods such as crystal interferometry,¹ analyzer-based imaging,² and free-space propagation (FSP)³ provide excellent performance, their high coherence requirements have restricted their use to synchrotron environments (or microfocal x-ray tubes), therefore limiting their commercial translation. Instead, both grating interferometry⁴ and edge illumination (EI)⁵ can be adapted to conventional laboratory sources.^{6,7} Our group has been focussing on the latter, for reasons related to its full achromaticity,⁸ compatibility with non-microfocal lab-sources without requiring a source grating,^{7,9} and tolerance to misalignment/vibration of the optical elements.^{10,11} Full details on the image formation principles in EI can be found in Refs. 12 and 13. While non-micro-focal sources can be used, EI’s basic principle requires that the beamlets created by the pre-sample mask do not mix,¹⁴ which still imposes a degree of limitation on the maximum focal spot that can be used. The projected focal spot convolved with the magnified aperture in the pre-sample mask must lead to a degree of smearing largely contained within a single pixel. For this reason, EI setups currently under development at University College London use high-powered x-ray sources (e.g., Rigaku M007) which, while being an excellent match with EI’s requirements¹⁵ due to their capability to generate high fluxes from focal spots around 70–100 μm , are high-end scientific instruments and therefore not particularly cost effective, which could be an aspect to consider in terms of commercial translation. Moreover, with the exception of targeted microscopy experiments,¹⁶ overall setup lengths so far ranged between 1.5 and 2 m.¹⁴

Here, we present an alternative implementation of the EI method that simultaneously allows the use of cheaper x-ray

sources, and the realisation of more compact setups. It is based on the introduction of a third x-ray mask, in close proximity to the source, analogous to the introduction of the source grating in Talbot-Lau grating interferometry setups.⁶ However, two significant differences should be noted. First, in grating interferometry, the source grating is used to increase coherence. Conversely, EI is an incoherent XPCI method^{9,18} and maintains this key characteristic also in this new implementation: the apertures in the source mask are large, and their only function is to allow the use of a much larger focal spot, since this could provide a more cost effective way to generate a sufficiently high x-ray flux. While in principle source apertures as large as 70–100 μm could be used, we used smaller apertures in this proof-of-concept experiment (17 μm), because we wanted to simultaneously investigate the possibility to reduce the overall system length. The angular sensitivity decreases with increased focal spot (above a given threshold) and reduced propagation distance.¹⁵ The latter has a direct influence on the overall system length, due to the need to limit the dimensions of the projected focal spot. Hence, the use of a smaller source should offset that of a reduced system length, while maintaining the same sensitivity. It should be noted that the apertures were still sufficiently large as to not generate any noticeable coherence effect. The second key difference from Talbot-Lau has to do with the effect that the source mask has on the acquired images. The one-to-one relationship between apertures in the sample/detector masks and detector pixels means that the use of multiple sources results in the generation of a plurality of images shifted by one pixel with respect to the other, with the number of images matching the number of sources. This is exemplified in Fig. 1 for the 3-source case. As a consequence of the above, the intensity $I(i)$ recorded by the i -th detector pixel is given by the contribution of the three sources, and can be expressed by the following relationship:

^{a)}Electronic mail: dario.basta.13@ucl.ac.uk



$$I(i) = \sum_{n=-1}^1 I_n(i), \quad (1)$$

where n indicates the source number (0 being the central one) and $I_n(i)$ is the intensity produced by the n -th source in the i -th pixel. Under the hypothesis that all sub-sources have the same shape but are just laterally shifted one respect to the other, $I_n(i)$ is equal to the intensity $I_0(i-n)$ produced by the central source in the $(i-n)$ -th pixel. Equation (1) can then also be written as

$$I(i) = \sum_{n=-1}^1 I_0(i-n). \quad (2)$$

By exploiting the properties of the Kronecker symbol $\delta_{i(n-j)}$, we can write Eq. (2) as

$$\begin{aligned} I(i) &= \sum_{n=-1}^1 \sum_j I_0(j) \delta(i-n-j) \\ &= \sum_j I_0(j) \sum_{n=-1}^1 \delta(i-n-j) \end{aligned} \quad (3)$$

by taking into account that the sum over j index is independent from the sum over n . By defining a Discrete Source Distribution (DSD) as $DSD(i) = \sum_{n=-1}^1 \delta(i-n)$ and exploiting the definition of discrete convolution

$$I(i) = \sum_j I_0(j) DSD(i-j), \quad (4)$$

so that the intensity in the i -th pixel is given by the discrete convolution of the intensity I_0 produced by one source in the center of the distribution and the DSD .

We explored the validity of the above approach through a combination of simulation work and a proof-of-concept experiment. Since a large focal spot was not available, we created one by defocusing the micro-focal source previously used for our microscopy studies¹⁶ where, however, the tungsten target was replaced with a molybdenum one. The source featured a $10\ \mu\text{m}$ thick transmission Mo target and was operated at 50 kV and 0.2 mA. While this is a transmission-type source that would normally allow reaching focal spots of $3\text{--}4\ \mu\text{m}$, in this case it was defocused to $>250\ \mu\text{m}$, allowing the production of three sources via a $150\ \mu\text{m}$ thick gold mask with a pitch of $98\ \mu\text{m}$ and $17\ \mu\text{m}$ apertures. A downside of this is the low emitted flux, since the source does not allow increasing the current above 0.2 mA; coupled to the use of an indirect conversion, passive-pixel CMOS-based flat panel detector (Hamamatsu C9732DK), this resulted in a noise level much higher than normally observed in EI experiments. However, this sub-ideal setup was sufficient to show that the approach works, and the agreement with the simulation supports the reliability of the obtained results. In particular, it should demonstrate that the sensitivity model described in Ref. 15, which allows maintaining a constant sensitivity by simultaneously reducing system length and focal spot size, still holds. This will be validated experimentally in future developments, along with possible tradeoffs between available flux and cost of existing x-ray sources with extended focal spots.

The detector mask matched the source mask design, apart from the aperture size, which was $29\ \mu\text{m}$ instead of $17\ \mu\text{m}$.

This imposes the use of a symmetrical set up for the pre-sample mask (see Fig. 1), in analogy to the set up first introduced in Ref. 17 in the context of grating interferometry. We used a mask with $48\ \mu\text{m}$ pitch, $15\ \mu\text{m}$ apertures, and $30\ \mu\text{m}$ gold nominal thickness, previously used in Ref. 19. Harmonic matching was then obtained through a small rotation of the source and detector mask to slightly reduce their effective pitch. This enabled a significant system length reduction while maintaining a propagation distance and a projected source size very close to those used in previous systems, where a $70\ \mu\text{m}$ focal spot was demagnified 4 times by the 1.6/0.4 source-to-sample/sample-to-detector distance arrangement.^{7,9,14} All masks were aligned by means of the compact system described in Ref. 20. Inter-mask distances were of 0.5 m, for an overall system length of 1 m. The thin gold layer of the sample mask is another non-ideal parameter affecting the ultimate image quality.

The same parameters used in the experiment were implemented in the simulation based on a wave optics model,²¹ and example results are provided for a wire sample with a diameter of $400\ \mu\text{m}$. In Fig. 2, we show both “undithered” (Fig. 2(a) vs Fig. 2(b)) and “dithered” (Fig. 2(c) vs Fig. 2(d)) intensity profiles of EI differential phase-contrast images; with “dithering,” we refer to a procedure in which the spatial resolution in the final image is increased by re-combining multiple frames acquired while the sample is displaced by sub-pixel positions.^{14,19,22}

In this case, 6 sub-pixel steps were used. As can be seen, while going from a single source to three sources simply broadens the peaks in the undithered profiles (Fig. 2(a) vs Fig. 2(b)), the effect is markedly different in dithered ones. In the latter case, the use of three sources results in three distinct positive and negative peaks: these are effectively three separate image profiles, each one created by one of the three “sourcelets” shifted by the number of dithering steps. However, images equivalent to those created by a single source can be restored by inverting Eq. (3), which can be done by means of a

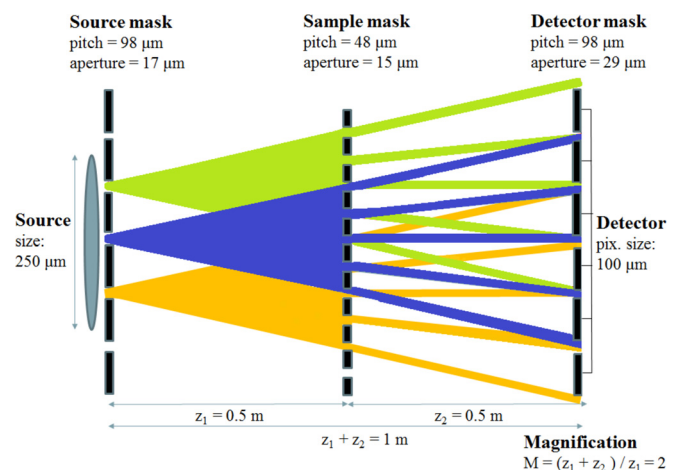


FIG. 1. Schematisation of the experimental setup. Different colours have been used for different sub-sources defined by an aperture in the source mask. Each one creates an image shifted by one detector pixel with respect to its neighbours. While the illumination of five pixels from each source is displayed for demonstration purposes, this actually extends over the entire field of view.

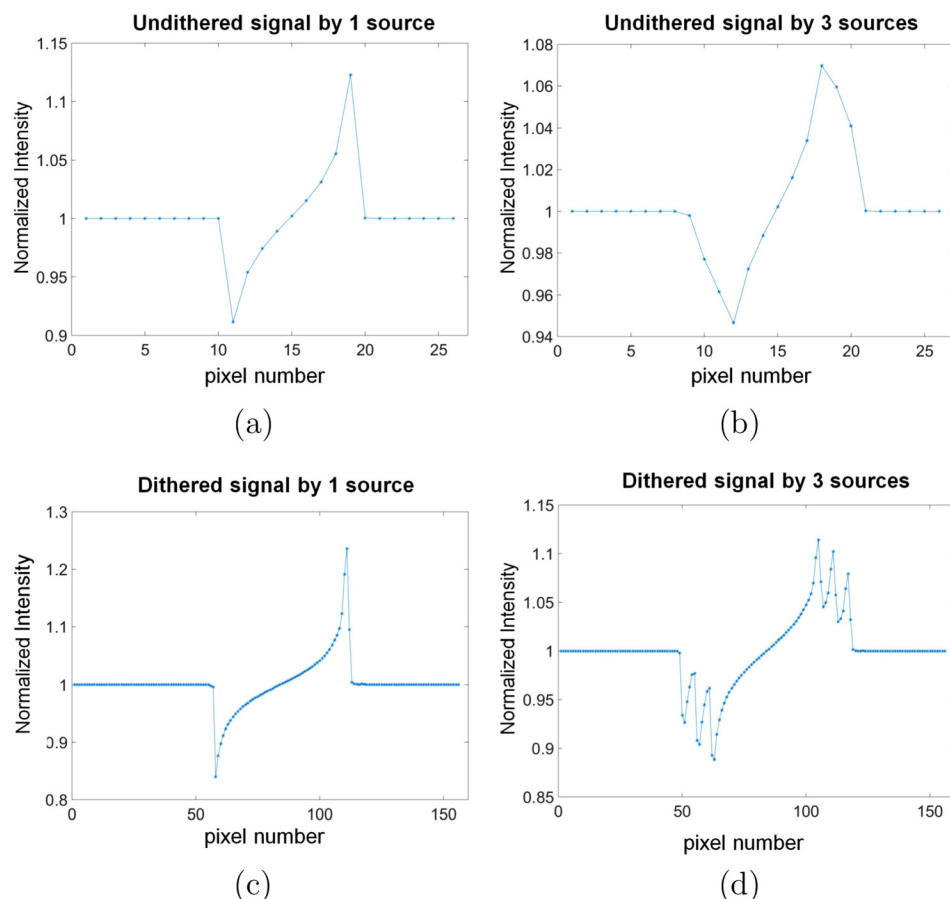


FIG. 2. Comparison between simulated intensity profiles of EI differential phase-contrast images of a wire sample, generated by using one source (a) and (c) and three sources (b) and (d); (a) and (b) represent “undithered” profiles; (c) and (d) “dithered” ones. In the labels of the horizontal axes, we refer to “image” pixels, rather than physical detector pixels: these correspond to the detector pixel size in undithered images, and to detector pixel size divided by the number of dithering steps in the dithered ones. Note also that the signal intensity is higher in the dithered cases, thanks to the finer sampling of the peak near its maximum value.¹⁹ For all plots, the intensity normalised through division by the number of counts in the background is plotted as a function of the pixel number.

deconvolution procedure. In this case, we used the Richardson-Lucy algorithm with a total variation regularization.²³

A key test on the simulation is the reproduction of the illumination curve, i.e., the curve obtained in the absence of the sample when the sample mask is scanned over one period in the direction transverse to the mask apertures. In this experiment, the illumination curve was also used to check the alignment since, if harmonic matching is not perfectly achieved, the illumination curve would be broadened. Figure 3 shows the comparison between simulated (solid line) and experimental (circles) illumination curves and a good agreement can be observed.

Experimental images of geometrical objects are shown in Fig. 4. Cylindrical fibres featuring both high (Sapphire, diameter $250\ \mu\text{m}$) and low (Polybutylene Terephthalate (PBT), diameter $180\ \mu\text{m}$) absorption and phase shifts were used; experimental acquisitions were performed with 12 dithering steps of $4\ \mu\text{m}$ step size and exposure time of approximately 1000 s per position. The acquired images were subsequently deconvolved with the Lucy-Richardson procedure. All the images are mixed intensity projections, obtained by illuminating only one side of the detector pixels with 50% of the total intensity (corresponding to one side of the illumination curve). The agreement with the simulation provides confidence that extension to quantitative phase retrieval⁹ and to dark field imaging²⁴ can be applied to these images, just as done previously for “standard” EI images. These developments go beyond the scope of the current proof-of-concept study and will be explored in future work. Two things can be noted: (1) the deconvolution procedure restores the expected “single

positive/single negative” peak typical of differential phase contrast profiles, while at the same time restoring the higher peak intensity that would be produced by a single source, and (2) a good agreement between simulation and experiment was obtained for both the acquired and the deconvolved profiles, which in Figs. 4(d) and 4(h) are compared with theoretical profiles generated by a single source. This last aspect is particularly important, because it proves that the deconvolution procedure is capable of restoring images that would be created by a single source. The remaining small oscillations around the main peaks are due to cross-talk between pixels,^{14,19} indeed,

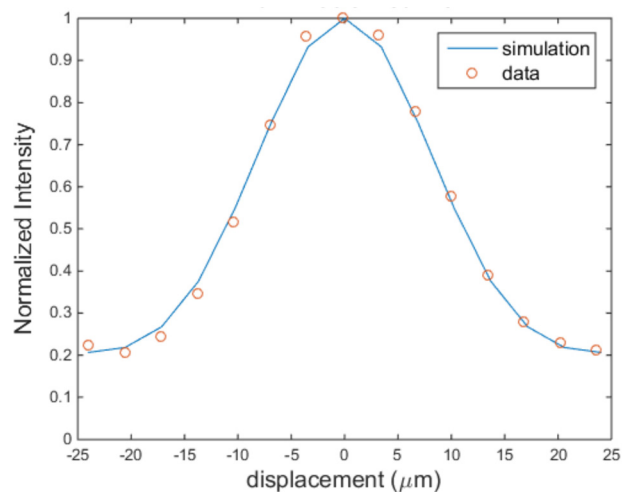


FIG. 3. Simulated (solid line) vs experimental (circles) illumination curves. The 20% offset in both curves is due to the relatively high transmission through the thin sample mask.

they are also present in profiles simulated through the use of a single source. Note that cross-talk had not been added to the simulated profiles shown in Fig. 2, since in that case we were interested in understanding the signal behaviour under “ideal” conditions. All images were obtained with the pre-sample mask placed in the position corresponding to the maximum slope in the illumination curve, i.e., to a normalised intensity of approximately 0.6 (see Fig. 3).

Finally, in order to test the approach on a more complex biological sample, we acquired images of a ground beetle, with the same setup and imaging conditions described above. Acquired and deconvolved images are shown in Figs. 5(a) and 5(b), respectively. Also in this case, the three differential phase contrast peaks are restored to one (see arrows), and their intensity is enhanced. Additional peaks of lower intensity can be attributed to cross-talk, as discussed previously.

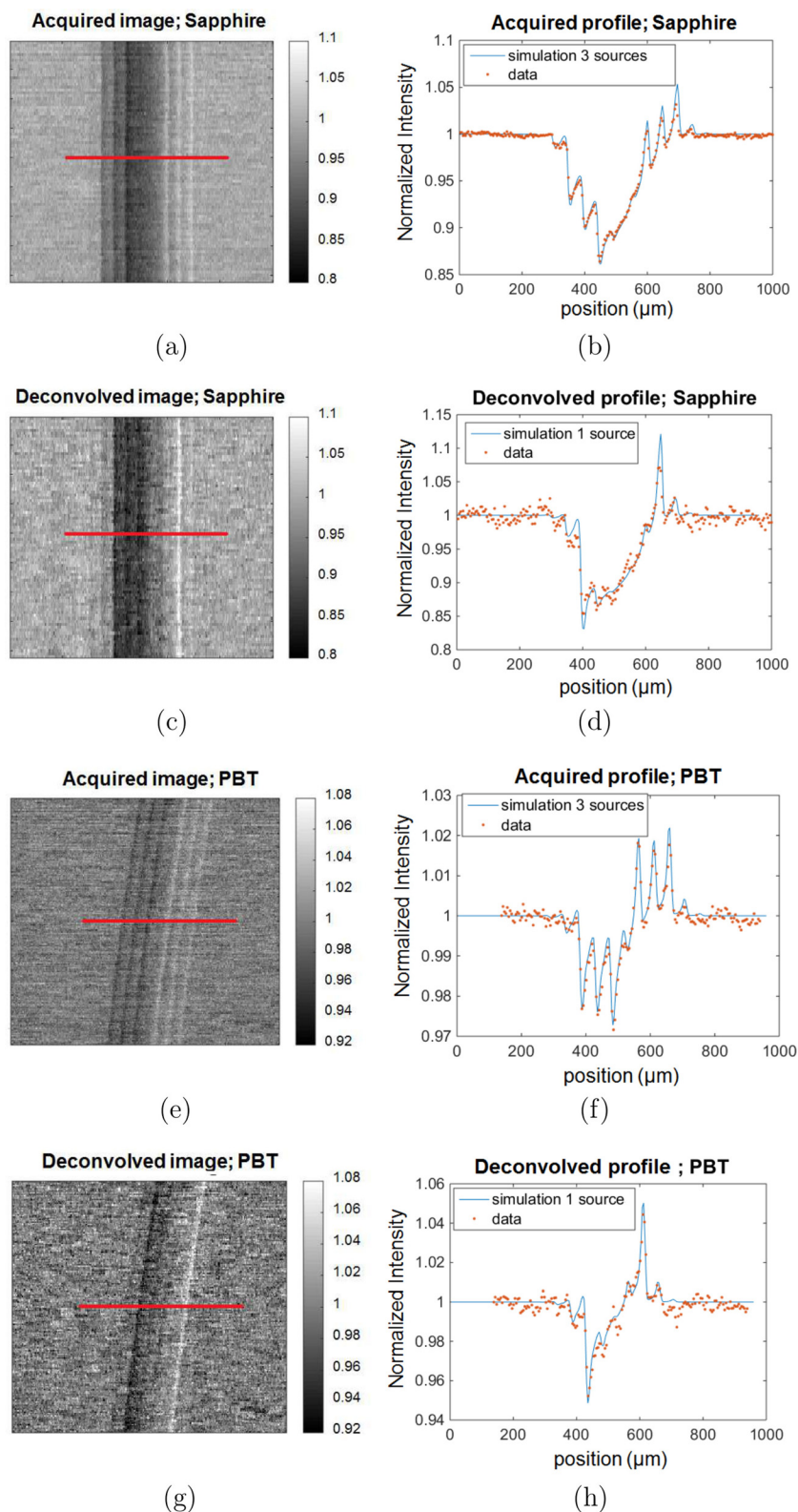


FIG. 4. Dithered images of cylindrical fibres made of sapphire ((a) acquired and (c) deconvolved) and PBT ((e) acquired and (g) deconvolved). Corresponding image profiles along the pixel rows indicated by the solid red lines across the images ((b) sapphire acquired, (d) sapphire deconvolved, (f) PBT acquired, and (h) PBT deconvolved)). For all profiles, solid lines represent the simulation and dots experimental values.

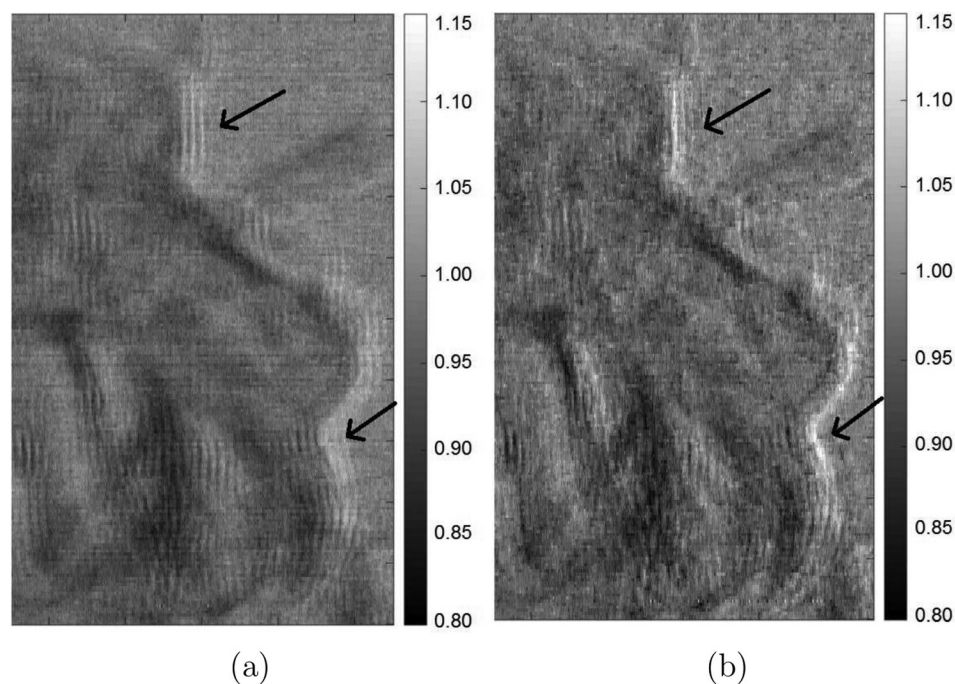


FIG. 5. Acquired (a) and deconvolved (b) images of a ground beetle. The right part of the head is shown to underline how the three peaks in the recorded image are restored to a single, more intense one in the deconvolved image (see arrows).

In summary, we have performed a proof-of-concept study to demonstrate that segmenting a large focal spot x-ray source through an appropriate mask is a viable approach in EI XPCI. While in principle it would be possible to create sub-sources as large as $100\ \mu\text{m}$, the creation of smaller sources offers the opportunity to reduce system dimensions. This aspect was also explored in this proof-of-concept study, by building and evaluating a system with an overall length of 1 m. The use of several sub-sources results in the creation of multiple, spatially shifted images, which need to be disentangled by means of appropriate algorithms. In this context, good results were obtained by using the Richardson-Lucy deconvolution method with a total variation regularization. One important aspect of future studies will be the assessment of whether the deconvolution procedure affects image quality. It should be noted however that positive indications on the effectiveness of similar approaches have already been provided for FSP.^{25,26} While the non-ideal nature of the used proof-of-concept setup (especially low flux and thin pre-sample mask) resulted in limited signal-to-noise ratio, the experiment was sufficient to prove that the proposed approach works, and provides results which are in agreement with our simulation framework. Future work will investigate the extension of this concept through the design of optimised systems, especially in terms of, e.g., maximum number of sources that could be used and minimum system dimensions.

This work was supported by the UK Engineering and Physical Sciences Research Council Grant No. EP/I021884/1 and by the UK Science and Technology Facilities Council Grant No. ST/L502662/1. M.E. is supported by Marie Curie Career Integration Grant within the Seventh Framework Programme of the European Union PCIG12-GA-2012-334056. A.A. is supported by a project funded under the Innovative Research Call in Explosives and Weapons Detection 2013 initiative. This is a Cross-Government Programme sponsored under the UK Governments CONTEST strategy in partnership

with the U.S. Department of Homeland Security, Science and Technology Directorate.

- ¹U. Bonse and M. Hart, *Appl. Phys. Lett.* **6**, 155 (1965).
- ²T. Davis, D. Gao, T. Gureyev, A. Stevenson, and S. Wilkins, *Nature (London)* **373**, 595 (1995).
- ³A. Snigirev, I. Snigireva, V. Kohn, S. Kuznetsov, and I. Schelokov, *Rev. Sci. Instrum.* **66**, 5486 (1995).
- ⁴C. David, B. Nöhhammer, H. Solak, and E. Ziegler, *Appl. Phys. Lett.* **81**, 3287 (2002).
- ⁵A. Olivo, F. Arfelli, G. Cantatore, R. Longo, R. Menk, S. Pani, M. Prest, P. Poropat, L. Rigon, G. Tromba, E. Vallazza, and E. Castelli, *Med. Phys.* **28**, 1610 (2001).
- ⁶F. Pfeiffer, T. Weitkamp, O. Bunk, and C. David, *Nat. Phys.* **2**, 258 (2006).
- ⁷A. Olivo and R. D. Speller, *Appl. Phys. Lett.* **91**, 074106 (2007).
- ⁸M. Endrizzi, F. A. Vittoria, G. Kallon, D. Basta, P. C. Diemoz, A. Vincenzi, P. Delogu, R. Bellazzini, and A. Olivo, *Opt. Express* **23**, 16473 (2015).
- ⁹P. R. T. Munro, K. Ignatyev, R. D. Speller, and A. Olivo, *Proc. Natl. Acad. Sci. U. S. A.* **109**, 13922 (2012).
- ¹⁰T. Millard, M. Endrizzi, K. Ignatyev, C. Hagen, P. R. T. Munro, R. D. Speller, and A. Olivo, *Rev. Sci. Instrum.* **84**, 083702 (2013).
- ¹¹M. Endrizzi, D. Basta, and A. Olivo, *Appl. Phys. Lett.* **107**, 124103 (2015).
- ¹²A. Olivo and R. D. Speller, *Phys. Med. Biol.* **53**, 6461 (2008).
- ¹³P. C. Diemoz and A. Olivo, *Opt. Express* **22**, 28199 (2014).
- ¹⁴A. Olivo and R. D. Speller, *Phys. Med. Biol.* **52**, 6555 (2007).
- ¹⁵P. C. Diemoz, C. K. Hagen, M. Endrizzi, and A. Olivo, *Appl. Phys. Lett.* **103**, 244104 (2013).
- ¹⁶M. Endrizzi, F. A. Vittoria, P. C. Diemoz, R. Lorenzo, R. D. Speller, U. H. Wagner, C. Rau, I. K. Robinson, and A. Olivo, *Opt. Lett.* **39**, 3332 (2014).
- ¹⁷T. Donath, M. Chabior, F. Pfeiffer, O. Bunk, E. Reznikova, J. Mohr, E. Hempel, S. Popescu, M. Hoheisel, M. Schuster, J. Baumann, and C. David, *J. Appl. Phys.* **106**, 054703 (2009).
- ¹⁸A. Olivo, K. Ignatyev, P. R. T. Munro, and R. D. Speller, *Appl. Opt.* **50**, 1765 (2011).
- ¹⁹K. Ignatyev, P. R. T. Munro, R. D. Speller, and A. Olivo, *Rev. Sci. Instrum.* **82**, 073702 (2011).
- ²⁰D. Basta, M. Endrizzi, F. A. Vittoria, G. K. N. Kallon, T. P. M. Millard, P. C. Diemoz, and A. Olivo, *Rev. Sci. Instrum.* **86**, 096102 (2015).
- ²¹F. A. Vittoria, P. C. Diemoz, M. Endrizzi, L. Rigon, F. C. Lopez, D. Drossi, P. R. T. Munro, and A. Olivo, *Appl. Opt.* **52**(28), 6940 (2013).
- ²²P. C. Diemoz, F. A. Vittoria, and A. Olivo, *Opt. Express* **22**, 15514 (2014).
- ²³W. Richardson, *J. Opt. Soc. Am.* **62**, 55 (1972).
- ²⁴M. Endrizzi, P. C. Diemoz, T. P. Millard, J. L. Jones, R. D. Speller, I. K. Robinson, and A. Olivo, *Appl. Phys. Lett.* **104**, 024106 (2014).
- ²⁵A. Olivo and R. D. Speller, *Phys. Med. Biol.* **54**, N347 (2009).
- ²⁶L. De Caro, F. Scattarella, S. Tangaro, D. Pelliccia, C. Giannini, U. Bottigli, and R. Bellotti, *Med. Phys.* **38**, 1951 (2011).